A Form Tolerancing Theory Using Fractals and Wavelets

R. S. Srinivasan[1]

K. L. Wood
Associate Professor.

Department of Mechanical Engineering,
The University of Texas,
Austin, TX 78712

Tolerancing is a crucial problem for mechanical designers, as it has quality and cost implications on product design. Research in tolerancing has addressed specific areas of the problem, but lacks a theoretical basis. A formal approach for geometric tolerancing with fractal-based parameters has been recently developed. This paper presents an enhanced error profile analysis and synthesis method, based on wavelets, that maintains and extends the use of fractals for surface error abstraction. An overview of the theory of wavelets is provided, and the link between fractals and wavelets is established. Physical test data are used to illustrate the application of wavelet theory to surface profile reconstruction and synthesis. The synthesis methods are then implemented in the functional design of ball-bearing elements, demonstrating the utility of fractal-based tolerancing. Plans for further study and implementation conclude the paper.

1 Introduction

The scope of mechanical design has expanded considerably in the last decade, as designers are faced with the demand for higher quality products, and shorter turn-around time from design to market. The demand for higher quality and reliable performance has strong links to the *precision* of the products. The designer must specify the allowable limits on manufacturing error, so that function is not impaired and so that cost is maintained at a minimal level. These limits on the error of manufactured parts are called *tolerances.*

With respect to the engineering disciplines, tolerances assume a variety of meanings. We are primarily interested in mechanical tolerances applied to physical-product features, such as machined parts and assemblies. Mechanical tolerances, in this sense, are basically categorized as:

- **Size Tolerances:** control the error on the overall size of a particular feature, e.g., length of a pipe or diameter of a shaft.
- **Geometric Tolerances:** specify permissible deviations in the geometric characteristics of the part or feature, e.g., straightness of the axis of a pipe or circularity of a shaft. Geometric tolerances refine the size tolerances to exercise a closer control over form and function. Geometric tolerances conform to the ANSI Y14.5M standards, and are subclassified into form, orientation, location, and runout tolerances (Walker and Srinivasan, 1993). This paper is restricted to the study of the form tolerance subset.

Current industrial practices to assign tolerances are usually based on highly specialized experimentation or experience. One of the major tolerancing impediments lies in establishing a clear link between tolerance specification and part function. Without such a link, costly production errors can result, leading to rework, part rejection, and increased manufacturing scrap. The need is thus paramount to develop *general* geometric tolerancing techniques that emphasize the function-tolerance relationship.

1.1 The Tolerance-Function Connection in Mechanical Design. The inter-relationship between tolerances or submacrogeometric errors and the functionality of machine elements remains poorly defined and understood (Tipnis, 1992). The elucidation of such a relationship is a pressing need in the modern context of advances in materials and manufacturing technology (Tumer, Srinivasan, and Wood, 1995). New materials processing and manufacturing techniques pave the road for achieving high precision in machine components. For example, the Rolls-Royce company predicts a significant increase in gearbox capacity for aerospace geared power transmissions, with a reduction in the gear tooth composite error (McKeown, 1987). The same company also projects improved compressor efficiency, as a consequence of more accurate aerofoil profiles in the rotor and stator blades of axial compressors. While the predicted improvement in performance is promising, designers do not have the tools to specify, understand, and control the errors on machine elements, in a cost-efficient and effective manner. A rational basis is thus required for relating component errors to performance, without resorting to expensive trials.

1.2 Status of Tolerancing Research. The field of tolerance research contains a number of diverse and interesting problems: the assignment of tolerances in design, the assessment and control of the precision of manufacturing processes, the representation of tolerances in geometric models, metrological issues concerning the verification of tolerances, and cost-tolerance-quality interactions. Some of the important advancements such as virtual boundaries theory (Jayaraman and Srinivasan, 1989), and *M*-space theory (Turner and Wozny, 1990) have been discussed in the authors' earlier papers (Srinivasan and Wood, 1992a, 1992b, 1995).

As it will be impossible to review all the notable research contributions in this continually growing field, one approach from each of the above areas is described below to illustrate the trends of investigation. Zhang and Huq (1992), in a recent review paper, provide a wider coverage of the state-of-the-art tolerance theories and techniques.

Requicha (1983) has formulated the *offset boundaries* theory, which prescribes tolerance zones for surface features by generating inner and outer offsets of the nominal features. The theory further suggests a combination of individual feature offset boundaries to form a single offset boundary for a part. However, the *structure* of the errors within the tolerance zone and the link to manufacturing processes are not addressed. Taguchi formalized the quality-tolerance interaction, by defining quality in terms of a continuous loss to society as a function of departure from a target value. A more recent approach in this area is due to Vasseur et al. (1993), wherein product cost is linked to process accuracies and inspection methods. The emphasis is on

[1] Currently with Applied Materials, Inc., Austin, TX 78724

[†] Associate Professor, ETC 5.160, The University of Texas, Austin, TX 78712-1063

Contributed by the Design, Theory, and Methodology Committee for publication in the JOURNAL OF MECHANICAL DESIGN. Manuscript received July 1994; revised Aug. 1996. Associate Technical Editor: D. L. Thurston.

Table 1 Mathematical tools for trend and periodicity

Component	Detection	Model	Estimation
trend	• Autocorrelation: slow decay • Power Spectrum: peak at zero frequency	$y_t(x) = y_{t0} + s_t \cdot x$ y_{t0} = y-intercept s_t = slope	linear regression
periodic	• Autocorrelation: periodic • Power Spectrum: peak at underlying frequency	$y_p(x) = y_{p0} + d_a \cdot \sin(2\pi f_r x/L)$ y_{p0} = offset, d_a=amplitude f_r = frequency	nonlinear regression

the cost of the product, rather than synthesizing part models for design. In metrology-related research, Ge et al. (1992) have developed computer-integrated inspection modules for tolerance specification and verification, enabling the user to specify and modify tolerance information, and to evaluate the part with respect to a datum reference frame and a minimum zone of acceptance. However, the concept of a zone to define the errors is not necessarily a true indicator of part performance; e.g., the structure of the errors within the tolerance zone is also an important factor influencing the function (Srinivasan and Wood, 1992a). In research related to geometric modeling, Shah and Miller (1989) assign geometric tolerances to selected features, based on evaluated boundary entities. The assignment, however, does not consider part function explicitly. Li and Zhang (1989) introduce a tolerance control module in a CAPP system, to automatically calculate dimensions and tolerances for each step in a machining process, using tolerance graphs. The focus is on tolerance control in machining, as opposed to tolerance design.

Most of the recent approaches deal with one of the above aspects of tolerance research, and some problems warrant such exclusive treatment, e.g., tolerance representation in solid models. However, in a recent mechanical tolerancing workshop, Tipnis (1992) indicates that "...*participants could not present any documented case studies as to why specific tolerances were chosen and how these tolerances were achieved*...". This statement reveals the emphasis of current researchers on the "fit" aspect of tolerances, rather than on the "functional" facet. The need thus exists for a formal theory and associated methods to assess the effect of tolerance scale errors on part performance, the precursor to assigning appropriate tolerances. This paper addresses this important area of modern design, building upon a proposed fractal-based approach to geometric tolerancing (Srinivasan and Wood, 1992b; Srinivasan, Wood, and McAdams, 1996; Srinivasan and Wood, 1995).

2 Complexity of Form Errors and Tolerances

In the course of machining a part, the machining system is subjected to a number of error sources (Srinivasan and Wood, 1992a). These errors are the result of complex physical mechanisms and possess a number of characteristics, e.g., trends, which are loosely interpreted as slopes, periodicities, etc. (Srinivasan, 1994; Whitehouse, 1978). The rich structure present in the errors calls for the use of an array of tools to identify the presence or absence of such components.

Assuming relative independence of the mechanisms causing the different structures, *a superposition model* for surface errors is used in this research:

$$y(x) = y_t(x) + y_p(x) + y_i(x), \tag{1}$$

where $y_t(x)$, $y_p(x)$, and $y_i(x)$ are the trend, periodic, and irregular components respectively. This model is in stark contrast to the existing concept of tolerance zones, where the *structure* of the profile within the zone is completely ignored. It is also the maiden application of a superposition model in mechanical tolerancing.

While Eq. (1) describes a general model for form errors, we need appropriate mathematical tools for abstracting the error in a minimal parameter set (*analysis*) and for generating realistic part models with these parameters (*synthesis*). Table 1 summarizes the tools and techniques used for the detection and estimation of the trend and periodic components. These methods are well established and described in the literature (Bendat and Piersol, 1966; Sen and Srivastava, 1990). The focus of this paper is on the irregular component, addressed using the novel concept of fractals.

2.1 Introduction to Fractals. The concept of fractals and fractal geometry have been engendered by Mandelbrot (1983), to describe irregular objects. Fractal objects are characterized by a non-integer dimension, called the *fractal dimension, D_f*. In the context of machined profiles, we represent the structure of manufacturing errors by a fractal dimension in the range from 1 to 2, with the fractional part of the dimension serving as a measure of the error. The fractal dimension is estimated from different scaling properties of the profiles. One such relationship is examined below.

The power spectrum of a signal (profile) is defined as the square of the magnitude of the Fourier transform. The spectrum of a fractal profile has an inverse power law relationship with the frequency (Mandelbrot, 1983):

$$S(\xi) \propto \xi^{-\beta(D_f)}, \tag{2}$$

where ξ is the frequency, and $\beta(D_f)$ is the spectral exponent, a function of the fractal dimension. This function is dependent on the value of the spectral exponent β, with different ranges of β corresponding to different models. Table 2 lists two ranges for β and their corresponding models and relations to the fractal dimension. Note that different notations are used for the two fractal dimensions to distinguish them from each other.

The authors have used properties similar to the above to develop a framework for fractal-based tolerances. The conceptual propositions have been tested through simulation for processes such as shaping in (Srinivasan and Wood, 1992a). A box counting algorithm is used to obtain the fractal dimension in the analysis of the simulated profiles. The potential utility of fractal tolerancing in mechanical design has also been demonstrated in (Srinivasan and Wood, 1992b). A fractional Brownian motion (fBm) method for generating profile errors is used to show the feasibility of fractal-based tolerances in the design of slider bearings.

2.2 Fractals and Wavelets. While the concepts of fractal dimension have proved useful for both analysis and synthesis of errors, the algorithms used for these purposes have their basis in different scaling properties of fractals. The box counting algorithm is based on the scaling property of covers, while the fBm is based on the scaling property of its increments (Mandelbrot, 1983; Srinivasan, 1994). This leads to inconsistencies in the fractal dimensions obtained from analysis, and those used for synthesis. Hence, a more robust model is needed that enables forward and inverse mapping of fractal-based error information. *Wavelet transforms* are presented in this paper as

Table 2 Relationship between fractal dimension and spectral exponent

β range	Model	Fractal Dimension
$1 < \beta < 3$	fractional Brownian motion	$D_f = 0.5(5 - \beta)$
$-1 < \beta < 1$	fractional Gaussian noise	$D_f^{\Delta} = 0.5(3 - \beta)$

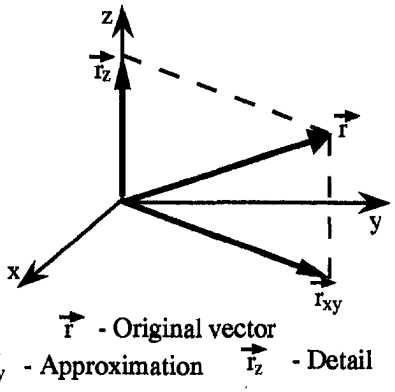

Fig. 1 Illustration of approximation and detail extraction operations

a suitable model for the analysis and synthesis of profile errors, since "...the theories of wavelets and fractals are mathematically interwoven and have aspects of striking resemblance"[2] (Srinivasan, 1994).

3 Multiresolution Analysis

Multiresolution analysis (Resnikoff, 1992; Chui, 1992; Mallat, 1989) provides the theoretical basis for implementing wavelet concepts in fractal-based tolerancing. The goal here is to use this analysis to develop, formally and rigorously, the link between wavelets and fractals.

3.1 Notation and Definitions. The central idea in multiresolution analysis is to examine a given signal or data sequence as successive approximations with an increased (or decreased) degree of smoothing. In our context, the data sequences are obtained from measuring the profile variations of machined surfaces. The name multiresolution analysis derives from the fact that the successive approximations correspond to different resolutions. The difference between two approximations is called the detail. The approximations are defined in *approximation spaces* and the details are described in corresponding *detail spaces.* To formalize these concepts, the following mathematical operations are needed.

The sets of integers and real numbers and complex numbers are denoted by $\mathbf{R}$ and $\mathbf{Z}$, respectively. An error profile of a mechanical surface (height variation) is denoted by a function $f(x)$, where x is the one-dimensional spatial variable. Since all machining errors are measurable and finite, formally, $f(x) \in L^2(\mathbf{R})$, which implies: $\|f\|^2 = \int_{-\infty}^{\infty} |f(x)|^2 dx < \infty$, where $\|f\|^2$ is the *norm* of the function $f(x)$. The *inner product* of two profile functions is defined as: $(f, g) = \int_{-\infty}^{\infty} f(x)\,\overline{g(x)}\,dx$ ($f, g \in L^2(\mathbf{R})$), where $\overline{g(x)}$ indicates the complex conjugate of $g(x)$. Prior to delving into wavelet mathematics, the concepts of approximations and details are illustrated using vectors and dot products.

3.2 Conceptual Aid. Consider Fig. 1. A three-dimensional vector space is shown, with a representative signal in this space denoted by the vector $\vec{r}$. The projection of $\vec{r}$ onto the xy plane is called $\vec{r}_{xy}$, and this forms the best "approximation" of $\vec{r}$ in the xy plane. The familiar dot product, used for the projection operation in vectors, is a simpler version of the inner product. Since the unit vectors $\vec{i}$ and $\vec{j}$ form an orthonormal basis for the xy plane, $\vec{r}_{xy}$ is expressed in dot product form as:

$$\vec{r}_{xy} = (\vec{r}, \vec{i})\vec{i} + (\vec{r}, \vec{j})\vec{j}. \tag{3}$$

In approximating $\vec{r}$ by $\vec{r}_{xy}$, the information lost is the z component or the height from the xy plane, i.e., $\vec{r}_z$. This forms the "detail" counterpart. The approximation operation can be carried out for one more step, e.g., by projecting $\vec{r}_{xy}$ on to the x axis, viz. $\vec{r}_x$. The complement, $\vec{r}_y$, forms the detail. With this introduction, we now proceed to review the essence of wavelet theory. More detailed reviews are presented in (Rioul and Vetterli, 1991; Mallat and Zhong, 1992).

3.3 The Approximation Operation. Using the mathematical operations defined above, we can construct the approximation space of multiresolution theory. Consider the approximation of the original profile signal $f(x) \in L^2(\mathbf{R})$ at a resolution 2^m, $m \in \mathbf{Z}$. This operation is denoted by $A_m f(x)$. Mathematically, A_m is the (orthogonal) projection of functions in $L^2(\mathbf{R})$ on a vector space $V_m \subseteq L^2(\mathbf{R})$, i.e., V_m is the approximation space corresponding to the resolution 2^m, and contains all possible approximations of the function at this resolution. (Note that $A_m f(x)$ is the "best" approximation of $f(x)$ as it is the orthogonal projection.) Successive approximations define a family of approximation spaces $V_m \subseteq L^2(\mathbf{R})$, $m \in \mathbf{Z}$. The set of all approximation spaces (V_m) is called a *multiresolution approximation* of $L^2(\mathbf{R})$.

3.3.1 Approximation Basis Functions: Computation and Filters. Recall the definition of A_m as the orthogonal projection on the approximation space V_m. An orthonormal basis of V_m can be developed from the dilations and translations of a *scaling function* $\phi(x)$ (Mallat, 1989); i.e., the basis functions for V_m are formally defined as:

$$\phi_m^k(x) = \sqrt{2^{-m}}\phi_m(x - 2^{-m}k), \quad k \in \mathbf{Z} \tag{4}$$

where $\phi_m(x) = 2^m\phi(2^m x)$, $m \in \mathbf{Z}$. The *nesting property* of wavelets imposes a fundamental relationship between the bases of V_0 and V_1:

$$\phi(x) = \sqrt{2} \sum_{k=-\infty}^{\infty} a_k \phi(2x - k), \tag{5}$$

where $\{a_k\}$ are the coefficients of the scaling function. This is the two-scale dilation equation, and is true for any two successive approximation spaces (Daubechies, 1988).

The approximation of a function $f(x)$ (e.g., a surface profile) can be obtained in terms of the orthonormal basis defined above:

$$A_m f(x) = 2^{-m} \sum_{k=-\infty}^{\infty} (f(u), \phi_m(u - 2^{-m}k))\phi_m(x - 2^{-m}k). \tag{6}$$

Note the similarity between Eqs. (6) and (3). The above approximation is characterized by the coefficients in the decomposition; these coefficients are called the *discrete approximations* of the given function/signal $f(x)$ and are written as

$$(A_m^k f)_d = (f(u), \phi_m(u - 2^{-m}k)), \quad k \in \mathbf{Z}. \tag{7}$$

Since the above operations involve inner products, simpler equivalent expressions can be obtained by invoking the "filters" concept from signal processing. Filters are typically characterized by their *impulse response,* denoted h_k, which is the output corresponding to an impulse input. With a knowledge of the impulse response, the output y^k corresponding to any input x^k can be computed (Oppenheim and Schafer, 1989):

$$y^k = \sum_{n=-\infty}^{\infty} h_{k-n} x^n. \tag{8}$$

Additionally, it can be proved (Srinivasan, 1994) that,

$$(f(u), \phi_m(u - 2^{-m}k) = \sum_{n=-\infty}^{\infty} (\phi_{-1}(u), \phi(u - (n - 2k))) \times (f(u), \phi_{m+1}(u - 2^{-m-1}n)). \tag{9}$$

[2] From the Program Statement of *Wavelets and Fractals* Conference, May 1994, Pittsburgh, PA.

In this context, Eq. (6) may be interpreted in terms of filtering the signal with a low-pass filter (Mallat, 1989). Consider a discrete filter H with the following impulse response:

$$h_k = (\phi_{-1}(u), \phi(u - k)), \quad k \in \mathbf{Z}. \tag{10}$$

The mirror filter $\tilde{H}$ is defined as having the impulse response $\tilde{h}_k = h_{-k}$. Using this notation, and the results from Eqs. (8) and (9), Eq. (7) can be written as (Srinivasan, 1994):

$$(A_m^k f)d = \sum_{n=-\infty}^{\infty} \tilde{h}_{2k-n}(f(u), \phi_{m+1}(u - 2^{-m-1}n))$$
$$= \sum_{n=-\infty}^{\infty} \tilde{h}_{2k-n}(A_{m+1}^n f)_d. \tag{11}$$

Note that Eqs. (11) and (8) are similar. h_{2k-n} in Eq. (11) implies filtering at every other point, i.e., obtaining a coarse approximation (A_m) from a finer one (A_{m+1}). At this juncture, we have obtained a mathematical basis for describing an approximation to any signal $f(x)$. We now describe the detail space of a signal that is needed to reconstruct the signal from the approximation space.

3.4 The Extraction of Detail. The information obtained about a signal varies as it is approximated at different resolutions. The information lost when stepping from an approximation space V_{m+1} to another space V_m is called the detail. The detail is contained in a *detail space* W_m, defined as the complement space of V_m in V_{m+1} (Daubechies, 1988). Symbolically, this relationship is represented as,

$$V_{m+1} = V_m \oplus W_m. \tag{12}$$

The above result follows directly from the Projection Theorem (Anton, 1984).

3.4.1 Detail Basis Functions: Computation and Filters. In a development similar to that of the approximation space, the detail space can be generated by a function $\psi(x)$, called the *wavelet function,* defined as follows (Daubechies, 1988):

Definition 1 *For each ϕ with adequate decay and smoothness, the associated wavelet function is defined by*

$$\psi(x) = \sqrt{2} \sum_k (-1)^k a_{1-k} \phi(2x - k). \tag{13}$$

Defining $\psi_m(x) = 2^m \psi(2^m x)$, $m \in \mathbf{Z}$, then

$$\sqrt{2^{-m}} \psi_m(x - 2^{-m}k), \quad k \in \mathbf{Z} \tag{14}$$

forms an orthonormal basis of W_m. Other names used for the wavelet function are, *mother wavelet,* and *analyzing wavelet* (Meyer, 1987). The name "wavelet" derives from the conditions imposed on $\psi(x)$ (Meyer, 1987), i.e., $\psi(x) \in L^2(\mathbf{R})$, implying finite energy, and $\int_{-\infty}^{\infty} \psi(x)dx = 0$, indicating the presence of oscillations. Taken together, the above two conditions indicate that $\psi(x)$ is a small, oscillating waveform, a wavelet.

The detail extraction operator is denoted by D_m. Along the same lines as the development for the approximation operator, we can define the detail of a signal $f(x)$ at a resolution 2^m. We can also define the *discrete details* and apply the filter interpretation (Srinivasan, 1994), such that

$$g_k = (\psi_{-1}(u), \phi(u - k)), \quad k \in \mathbf{Z}. \tag{15}$$

and

$$(D_m^k f)_d = \sum_{n=-\infty}^{\infty} \tilde{g}_{2k-n}(A_{m+1}^n f)_d, \tag{16}$$

where $\tilde{g}_k = g_{-k}$, the impulse response of the mirror filter $\tilde{G}$.

Given a physical profile, Eqs. (11) and (16) constitute the decomposition of the profile into approximations and details respectively. The next logical step is to explore the reconstruction of the original signal from the decomposed data.

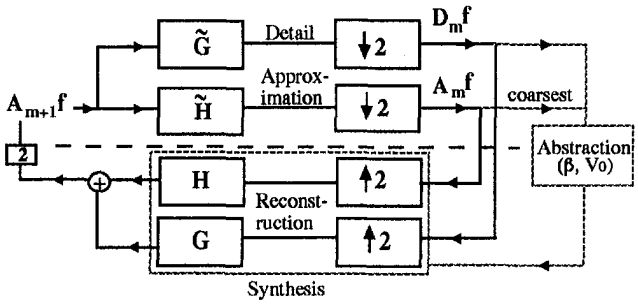

Fig. 2 Approximation, detail extraction, and reconstruction operations

3.5 Reconstruction of Profile. Following the implementation of the approximation and detail operators for surface profiles, a method is needed for reconstructing the profile signal. The reconstruction of the signal from the approximations and details is a natural consequence of the fact that V_m and W_m are orthogonal subspaces of V_{m+1} (Eq. 12). Hence $\sqrt{2^{-m}}\ \phi_m(x - 2^{-m}k)$, and $\sqrt{2^{-m}}\ \psi_m(x - 2^{-m}k)$ form an orthonormal basis for the space V_{m+1}. Using this property, the reconstruction formula is written in terms of the filtering operation by using the filter definitions in Eqs. (10), and (15) (Srinivasan, 1994):

$$(A_{m+1}^k f)_d = 2 \sum_{n=-\infty}^{\infty} h_{k-2n}(A_m^n f)_d + 2 \sum_{n=-\infty}^{\infty} g_{k-2n}(D_m^n f)_d. \tag{17}$$

The three operations, i.e., approximation, detail extraction, and reconstruction, are illustrated in Fig. 2. The procedures are shown in terms of the "filters" interpretation. $A_{m+1}f$ represents the signal at resolution $m + 1$. This is decomposed into approximation $A_m f$, and detail $D_m f$, by passing it through the filters $\tilde{H}$ and $\tilde{G}$, respectively. The $\downarrow 2$ implies that the approximation and the detail will possess only half the number of points as the original signal. The reconstruction can also be similarly interpreted, the difference being that the reconstruction will have twice as many points as the detail or approximation, and different filters are used, as indicated above.

The next section describes a metrological analogy to multiresolution analysis, drawn from the measurement of surface profiles.

3.6 Analogy: A Metrological Forerunner to Multiresolution Analysis. The central idea of multiresolution analysis is the representation of the profile or signal at various resolutions. A similar concept has been in vogue for the measurement of machined profiles, to quantify roughness and to separate roughness from waviness and form errors. This system of measurement is called the Envelope or E-system (Radhakrishnan, 1971; Whitehouse and Vanherck, 1972), wherein the following geometric procedure is used to construct "envelopes" of the total profile. Given the profile data, digitized at a high resolution, envelope profiles are generated by circles of different radii traversing the profile. The smaller the radius of the circle, the closer the envelope is to the original profile. As the radius increases, the envelope is dictated by the peaks in the profile (Fig. 3). The idea is to standardize the radius for effective separation of waviness. It is evident that the hierarchy of approximation operations corresponds to the construction of envelope profiles of varying radii, where the details can be interpreted as the difference in information between successive envelopes. The wavelet theory is thus symbolic of a *mathematical profiler,* analogous to a profile measurement instrument. Our vectorial interpretation in Section 3.2 and measurement analogy above serve to simplify the mathematical intricacies of wavelet theory to a more pragmatic level of a mathematical profiler.

4 The Link between Fractals and Wavelets

As indicated previously, both fractals and wavelets share the properties of non-stationarity and self-similarity. A number of

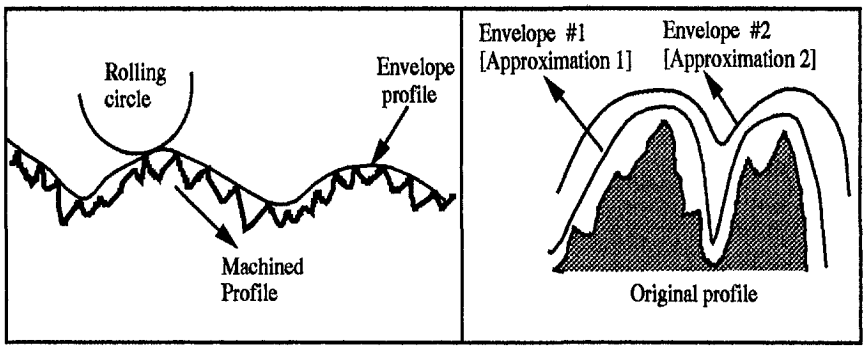

Fig. 3 The envelope system for profile measurement

researchers have examined this link more closely, notably Mallat et al. (1989, 1992), Wornell (1991), Arneodo et al. (1992), Muzy et al. (1994), and Farge et al. (1993). The approaches followed by the above authors use the common property of scale-dependence. Mallat and Wornell use the power spectrum method, which we extend in the next section.

Fractal profiles and surfaces are characterized by power spectra $S(\xi)$ of the form of Eq. (2). It can be shown that there exists a power law relationship between the variance of the details and the scale (Flandrin, 1992; Wornell, 1991). The proof uses the relationship between the power spectrum of the details at a given scale and the corresponding autocorrelation function, and hence the variance (Priestley, 1981). This scaling argument is expressed in terms of the variance of the discrete detail signals $(D_m^k f)_d$:

$$\sigma^2[(D_m^k f)_d] = V_0 2^{-\beta(D_f)m}, \tag{18}$$

where V_0 is a constant. With this equation, the fractal dimension is calculated from the slope of the log-log plot of the variance versus the scale 2^m. The parameter V_0 plays a crucial role in the total determination of the variance of the details, and hence the variational properties of the profile; it manifests as the y-intercept in the log-transformed version of Eq. (18). In the present context, we name it the "magnitude factor," as it represents the magnitude of a tolerance zone formed by a surface profile. In addition, the random process constructed with a set of mutually uncorrelated, zero-mean random variables, with variances as given in Eq. (18), yields a $1/f$ (fractal) profile.

5 Synthesis of Profiles from Fractal Parameters

The power-law relationship given by Eq. (18) provides a vehicle for the analysis of manufactured profiles and for the synthesis of "representative" profiles for the creation of realistic part models in design. We have used a typical profile from a grinding process to test the fidelity of the synthesis. The choice of a suitable scaling function $\phi(x)$, and the wavelet decomposition, reconstruction, and synthesis procedures are described below.

5.1 Scaling and Wavelet Functions. In order to implement the operations described above, appropriate scaling and wavelet functions are required. The simplest scaling function is the box function shown in Fig. 4(a). The corresponding wavelet function is the Haar function (Fig. 4(b)). It can be easily seen that the Haar function is a sum of dilates and translates of the box function. However, these functions possess discontinuities, and they influence the synthesis (Wornell, 1991). Hence, the choice of more regular basis functions is desirable. In this regard, Daubechies (1988) has developed families of scaling and wavelet functions, with increasing regularity. Regularity is related to the number of vanishing moments of the functions. It has been shown that as the regularity of the basis functions increases, the synthesis given by Eq. (18) is improved (Flandrin, 1992; Wornell, 1991). Based on these observations, we have chosen the scaling and wavelet functions with six vanishing moments; they have twelve coefficients for $\{a_k\}$ [defined in Eqs. (5) and (13)]. These coefficients are presented in Table 3; the derivation of these coefficients is described in (Daubechies, 1988). However, in order to compute the discrete approximations and details, the filter coefficients h_k and g_k are needed. The filter coefficients are related to $\{a_k\}$ as follows (Srinivasan, 1994):

$$h_k = a_k/\sqrt{2},$$

$$g_k = (-1)^k a_{3-k}/\sqrt{2}.$$

5.2 Reconstruction from Approximations and Details. One of the prime requirements of any tolerancing theory is that the actual tolerancing procedures must be made available to the user in a simple form, without the mathematical complexity (Tipnis, 1992). In this section we present the essentials of computation involved in the wavelet method.

A typical profile from a surface grinding process is used as a test case. The ground surface profile is measured using a profiling instrument. Long-wavelength errors, like trends, and periodicities, distort the fractal parameters (Stupak et al., 1992). Accordingly, the linear and periodic trends are removed using the tools in Table 1 and the superposition model, Eq. (1). The resulting profile used to demonstrate synthesis is shown in Fig. 5. The test profile data are available at 256 ($= 2^8$) discrete points, which constitute eight distinct scales. This is taken as the *base resolution* for the multiresolution analysis and is denoted by $2^{m=0} = 1$. The profile is decomposed into approximations and details at coarser resolutions, with each operation yielding half the number of points of the previous resolution. The approximations and details result from the convolution of a finer approximation with the scaling and wavelet coefficients respectively, using Eqs. (11) and (16). As the original profile

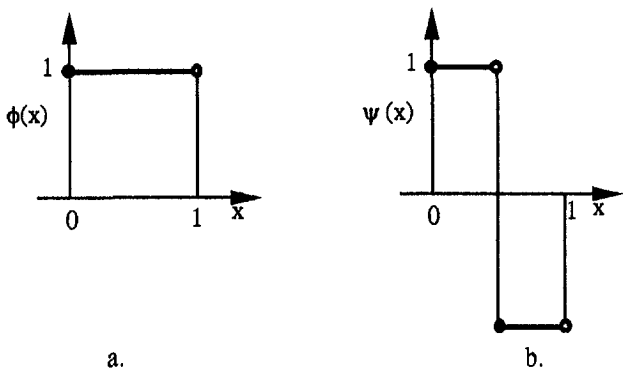

Fig. 4 Examples of scaling and wavelet functions: (a) box function (b) Haar function

Table 3 Coefficients a_k for Daubechies scaling and wavelet functions (Daubechies, 1988)

k	a_k
0	0.111540743350
1	0.494623890398
2	0.751133908021
3	0.315250351709
4	-0.226264693965
5	-0.129766867567
6	0.097501605587
7	0.027522865530
8	-0.031582039318
9	0.000553842201
10	0.004777257511
11	-0.001077301085

has 2^8 points, the decomposition (fine-to-coarse) is carried out to eight levels so that $(A^0_{-8}f)_d$ has only one point. We interpret this coarsest approximation as the mean height of the profile. However, as the profile has been detrended, the mean height is almost zero. Therefore, the original profile can be represented in terms of all the details corresponding to the range $(-8 \leq m \leq -1)$. The variance of the details at different scales is calculated and the fractal dimension computed from the slope of the log (*variance*) vs. log (*scale*) plot.

From the above representation, the approximations can be reconstructed (coarse-to-fine) using Eq. (17). The above operations result in perfect decomposition and reconstruction of the original signal; the result of the reconstruction of a test profile is shown in Fig. 5.

5.3 Synthesis. While the above reconstruction procedure is an important step, the main thrust of this research is to abstract the variational structure of machined profiles in a minimal parameter set. The power-law relationship given by Eq. (18) is at the heart of the abstraction. The variance of the details at each scale can be computed from a knowledge of D_f and V_0, which in turn are obtained from wavelet decomposition of the profile data. The discrete details are then generated as the samples of a zero-mean Gaussian process, with variance as calculated above. The coarsest approximation is assumed to be zero, typical of a de-trended and de-periodized signal. The approximations at successively finer resolutions are calculated using Eq. (17), until the approximation at the *base resolution* is obtained.

We verify the above synthesis procedure using a test profile from a grinding process. The height variations along a linear surface element are measured using a suitable profiling instrument. The horizontal resolution is selected as 0.1 *mm*, to accommodate the smallest diameter of the probes used for tolerance measurement (Wick, 1987). The number of data points is $N = 256$, to yield eight levels of resolution in wavelet analysis and synthesis; i.e., where resolution levels are in terms of 2^m, $-8 \leq m \leq -1$.

The original profile is assumed to be at a base resolution of 2^0, and decomposed to eight levels (i.e., $2^0 \rightarrow 2^{-8}$), to obtain the corresponding approximations and details. The coefficients to be used for these operations are obtained from the calculations outlined in Section 5.1. The variance of the details at each level is then calculated. This information is used to compute the fractal dimension and magnitude factor, using a linear regression on the logarithmic version of Eq. (18). The synthesis is carried out using these parameters, as described above. The result for the test profile is shown in Fig. 5, along with the reconstructed profile. The reconstruction is exact, and the synthesized profile reflects the structure and magnitude of errors in the original profile remarkably well. The energy and entropy of the test profile compared to the synthesized profile also show good agreement (Srinivasan, 1994).

6 A Design Example: Roundness of Ball Bearing Elements

A major advantage of fractal-based form tolerancing in comparison with other methods is that it facilitates study of the tolerance-function relationship (Srinivasan and Wood, 1992b). The theory of wavelets is perceived as an enhancement to the mathematical basis for fractal-based tolerancing. In order to illustrate the application of the theory outlined in this paper, a design example is presented.

Almost all systems of any technological significance have moving parts. These systems must use "bearing elements" to satisfy the functions of "support load" and "permit motion." We consider ball bearings here as our focus, in the context of a range of diverse applications, e.g., machine tool spindles, perambulator wheel axles.

In the design of any mechanical product, an important step is the estimation of the loads that are imposed on the device in service conditions. The problem considered here is the roundness errors in the rolling elements of ball bearings supporting the thrust load; these errors are a main source of vibration (Wardle, 1988). The designer has to exercise control on these geometric errors, by prescribing appropriate circularity tolerances. In current parlance (ANSI Y14.5M), this would mean prescribing a tolerance zone to delimit the deviations from an ideal circle. An alternative approach approximates the roundness errors as a sinusoidal wave around the circumference. Both approaches disregard the true structure of the errors. The approach presented below estimates the linear, periodic, and fractal components and combines them using the superposition model [Eq. (1)] (Tumer et al., 1995; Srinivasan et al., 1996).

6.1 Analysis of Bearing Forces. The important components of a ball bearing are shown in Fig. 6. Specifically, this is an angular-contact ball bearing, which can carry combined axial (thrust) and radial loads (Wardle, 1988; Srinivasan, 1994). The additional assumptions made in calculating bearing forces are: the bearing has N_b equispaced balls, firmly in contact with the

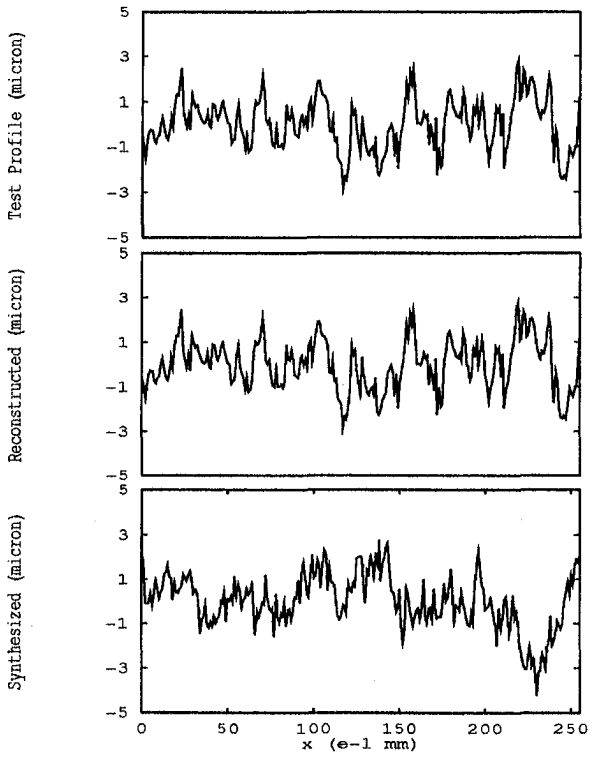

Fig. 5 Test, reconstructed, and synthesized profiles

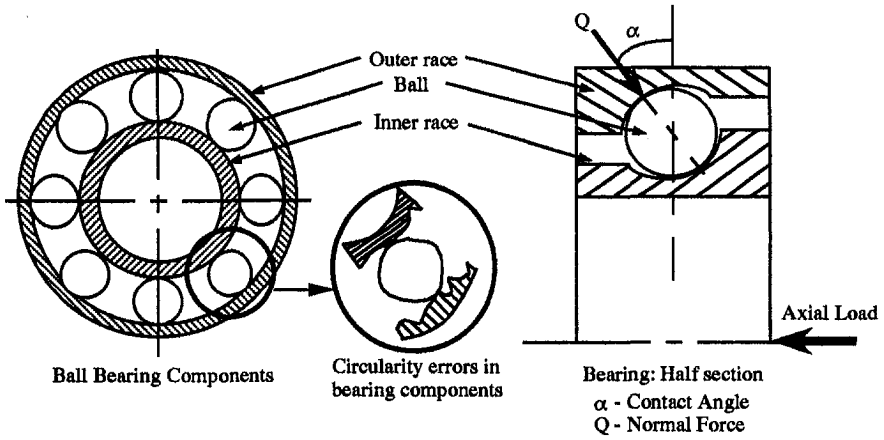

Fig. 6 Angular-contact ball bearing: geometry and forces

inner and outer races; the rotational speed of the bearing is moderate, implying negligible centrifugal forces; and the outer race is stationary.

The equations for the axial vibration force can be derived from the Hertzian contact forces. The normal load Q_i on a ball i can be written in terms of the corresponding deflection δ_i as:

$$Q_i = \kappa \delta_i^{3/2}, \quad 1 \leq i \leq N_b, \tag{19}$$

where κ is the contact compliance factor. The contact deflection δ_i is influenced by the geometric errors in the outer race, and is hence expressed as a nominal deflection δ_0 (i.e., in the absence of any geometric error) and a time-varying component $\delta_i(t)$, which is dependent on the relative position of the ball i and the outer race:

$$\delta_i = \delta_0 + \delta_i(t). \tag{20}$$

The contact compliance factor also changes due to $\delta_i(t)$. Thus Eq. (19) is approximated assuming a constant κ (Wardle, 1988):

$$Q_i = \kappa \delta_0^{3/2} \left\{ 1 + \frac{3\delta_i(t)}{2\delta_0} + \frac{3\delta_i^2(t)}{8\delta_0^2} \right\}. \tag{21}$$

The total axial force on the bearing is calculated from the sum of the axial components of the normal forces on all the balls (Fig. 6):

$$F_a = \sum_{i=1}^{N_b} Q_i \sin \alpha. \tag{22}$$

These equations are used in the calculation of axial vibration force for a test bearing. The data for the test bearing are adapted from (Wardle, 1988), and are furnished in Table 4.

Table 4 Relevant data for test bearing

Parameter	Value
Type	angular-contact
No. of balls	16
Ball diameter	1.40 mm
Pitch circle diameter	6.75 mm
Radial clearance	0.032 mm
Test load (axial)	1000 N
Test speed	1800 rpm
Contact deflection δ_0	0.0092 mm
Compliance factor κ	9.56×10^9 $Nm^{2/3}$
Contact Angle α	18.8°

Table 5 Trend and periodic parameters for test profiles

Test Profile	Trend Parameters		Periodic Parameters		
	s_t	y_{t0} (mm)	y_{p0} (mm)	d_a (mm)	f_r $(\times 256\ cps)$
Case 1	0.002408	1.142413×10^{-3}			
Case 2	0.012156	1.752679×10^{-3}			
Case 3			-0.004871	0.028065	29.345
Case 4			0.015253	-0.020047	29.265

6.2 Vibration Force with Synthesized Profiles. Equation (22) is used to calculate the axial force at various points in time, from $0 < t < T_0/N_b$, where T_0 is the time for one revolution of the bearing. For the purposes of this example, four test profiles generated from physical experiments are used to assess the impact of form errors on performance. The relevant superposition parameters (Table 1) from these cases are listed in Tables 5 and 6. An examination of the parameter values in the above tables shows a clear demarcation between Cases 1 and 2 and Cases 3 and 4. The former class of profiles exhibit linear trend only, along with lower values for the fractal parameters. Such profiles are typical of finishing processes without inherent periodicities, e.g., grinding. In contrast, the latter class has strong periodic trends, and higher values for the fractal parameters. These characteristics are found in roughing/semi-finishing processes, e.g., milling.

The fractal component of the overall profile is synthesized using the procedure outlined in Section 5.3. The complete profile is generated by adding the trend and periodic components to the fractal profile, as prescribed in Eq. (1). The synthesized profile is superposed on the ideal circumference of the outer race. Hence, the error at the point of contact augments the contact deflection of the ball; i.e., in Eq. (20) the error $\delta_i(t)$ is a contribution of the roundness error. Four different error profiles are synthesized, and the corresponding axial vibration forces are calculated from Eq. (22). The resulting force patterns are depicted in Fig. 7.

6.3 Comments on Test Results. A study of force patterns in Fig. 7 leads to some interesting observations. Cases 3 and 4 correspond to the higher values of the profile parameters, and, as

Table 6 Fractal parameters for test profiles

Test Profile	Fractal Parameters	
	D_f^A	V_0 (mm^2)
Case 1	1.247561	0.057347×10^{-6}
Case 2	1.271902	0.158817×10^{-6}
Case 3	1.880583	0.000041
Case 4	2.263826	0.000336

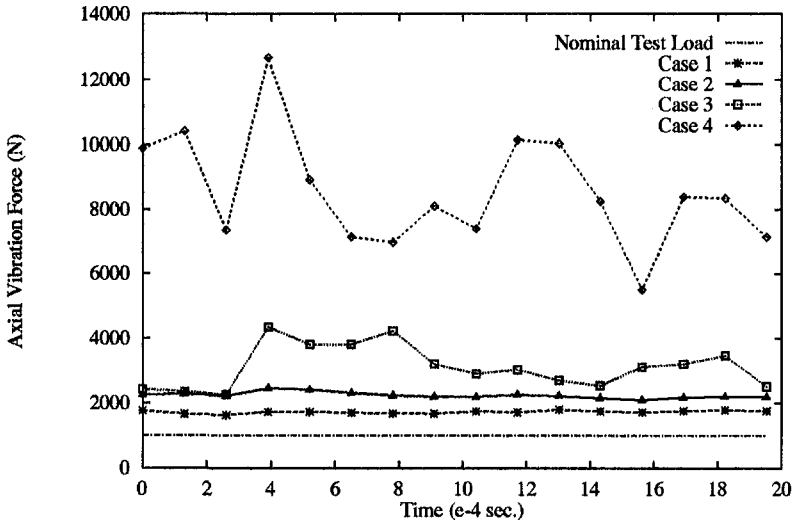

Fig. 7 Force patterns corresponding to various profiles

anticipated, the large contact deflections induce axial vibration forces well in excess of the nominal test load with large fluctuations. These results imply that a process like milling is inappropriate as a final process for the bearing outer race, as it is primarily a roughing or semi-finishing process. This can lead to excessively high contact stresses on the rolling elements. A finishing process is mandatory to control the error in the raceways. Cases 1 and 2 correspond to a finishing process with lower values for the profile parameters. The axial vibration forces are still larger than the nominal load, but the fluctuations are within a small band. The designer now has a reasonable basis to choose a finishing process, and the ability to choose between different manufacturing process parameters (e.g., Case 1 vs. Case 2), depending on the axial force requirements. A choice among process parameter combinations can also be dictated by the time to manufacture a part. Higher speeds and feeds result in higher volumetric material removal rates, and a compromise between acceptable performance and time to manufacture can be explored.

This simple design example illustrates that the proposed method can be a useful tool for the designer to assess the impact of different errors (manufacturing processes) on the performance of mechanical components.

7 Conclusion

The central idea of this work, i.e., using fractals for tolerancing, is novel. The theory of wavelets has been identified as an adjunct tool to compute the relevant fractal parameters. When combined with a novel superposition model of tolerances, a useful tool is made available in design for manufacturing.

One of the drawbacks of the current tolerancing standard, viz., ANSI Y14.5, is its lack of a formal mathematical basis. This paper presents a building block for a potential solution to this problem (Srinivasan, 1994; Srinivasan et al., 1996), focused on a mathematical abstraction of form errors. In accordance with this objective, the mathematics of wavelets and fractals has been described in some detail. However, for the benefit of practicing engineers, the essence of the theory is explained using vectors and dot products. The analogy with profile measurement also serves as another familiar backdrop to comprehend the practical aspects of the theory.

7.1 Future Work. The scope of investigation in this paper is limited to one-dimensional form tolerances. A natural extension is the development of the theory to encompass two dimensional form tolerances and eventually other geometric tolerances. Two dimensional irregular surfaces possess fractal dimensions in the range from 2 (no errors) to 3 (very irregular, volume-filling) (Mandelbrot, 1983). The requisite tools to perform the analysis and synthesis are more complex. A two-dimensional wavelet transform (Mallat, 1989) is a strong candidate.

Vectorial tolerances have been adopted by the ANSI Y14.5.1M standards (Walker and Srinivasan, 1993) to provide a mathematical representation of the tolerance zone. A major drawback is that statistical tolerancing is not incorporated. An appropriate representation of the fractal parameters would be a very efficient method of abstracting the variational information of manufacturing processes. Following further development of a suitable theory for geometric tolerances, the next step is the representation of the above tolerance parameters in a computational geometric model. This would make the mathematics latent, rendering the approach more accessible to practicing engineers.

8 Acknowledgments

This material is based upon work supported, in part, by The National Science Foundation, Grant No. DDM-9111372, an NSF Presidential Young Investigator Award, and research grants from Ford Motor Company, Texas Instruments, Desktop Manufacturing Inc, and the June and Gene Gillis Endowed Faculty Fellowship in Mfg.. Any opinions, findings, conclusions or recommendations expressed in this publication are those of the authors and do not necessarily reflect the views of the sponsors. The authors thank Dr. John E. Gilbert of the Department of Mathematics, at The University of Texas, for a number of useful discussions relating to wavelets.

References

Anton, H., 1984, *Elementary Linear Algebra* (4th edition), John Wiley & Sons, New York.

Arneodo, A., Argoul, F., Muzy, J. F., Pouligny, B., and Freysz, E., 1992, "The Optical Wavelet Transform," *Wavelets and Their Applications,* Ruskai, M. B., ed., pp. 241–273, Jones and Bartlett Publishers, Boston.

Bendat, J. S., and Piersol, A. G., 1966, *Measurement and Analysis of Random Data,* John Wiley & Sons, Inc., New York.

Chui, C. K., 1992, *An Introduction to Wavelets, Wavelet Analysis and its Applications,* Academic Press, Boston.

Daubechies, I., 1988, "Orthonormal Bases of Compactly Supported Wavelets," *Communications on Pure and Applied Mathematics,* Vol. XLI, No. 7, pp. 909–996.

Farge, M., Hunt, J. C. R., and Vassilicos, J. C., eds.., 1993, *Wavelets, Fractals, and Fourier Transforms,* Oxford University Press, New York.

Flandrin, P., 1992, "Wavelet Analysis and Synthesis of Fractional Brownian Motion," *IEEE Transactions on Information Theory,* Vol. 38, No. 2, pp. 910–917.

Ge, Q., Chen, B., Smith, P., and Menq, C. H., 1992, "Tolerance Specification and Comparative Analysis for Computer-Integrated Dimensional Inspection," *International Journal of Production Research,* Vol. 30, No. 9, pp. 2173–2197.

Jayaraman, R., and Srinivasan, V., 1989, "Geometric Tolerancing: Parts I and II," *IBM Journal of Research and Development,* Vol. 33, No. 2, pp. 90–124.

Li, J. K., and Zhang, C., 1989, "Operational Dimensional and Tolerances Calculation in CAPP System for Precision Manufacturing," *Annals of the CIRP,* Vol. 38, No. 1, pp. 403–406.

Mallat, S. G., 1989, "A Theory for Multiresolution Signal Decomposition: The Wavelet Representation," *IEEE Transactions on Pattern Analysis and Machine Intelligence,* Vol. 11, No. 7, pp. 674–693.

Mallat, S. G., and Zhong, S., 1992, "Characterization of Signals from Multiscale Edges," *IEEE Transactions on Pattern Analysis and Machine Intelligence,* Vol. 14, No. 7, pp. 710–732.

Mandelbrot, B. B., 1983, *The Fractal Geometry of Nature* (2nd edition), W. H. Freeman and Co., San Francisco.

McKeown, P., 1987, "The Role of Precision Engineering in Manufacturing of the Future," *Annals of the CIRP,* Vol. 36, No. 2, pp. 495–501.

Meyer, Y., 1987, "Orthonormal Wavelets," *Wavelets: Time-Frequency Methods and Phase Space,* Combes, J. M., ed., pp. 21–37, Berlin, Springer Verlag.

Muzy, J. F., Bacry, E., and Arneodo, A., 1994, "The Multifractal Formalism Revisited with Wavelets," *International Journal of Bifurcation and Chaos,* Vol. 4, No. 2, pp. 245–302.

Oppenheim, A. V., and Schafer, R. W., 1989, *Discrete-Time Signal Processing,* Prentice Hall, New Jersey.

Priestley, M. B., 1981, *Spectral Analysis and Time Series,* Vol. 1, Academic Press, Inc., London.

Radhakrishnan, V., 1971, "On an Appropriate Radius for the Enveloping Circle for Roughness Measurement in the *E*-System," *Annals of the CIRP,* Vol. 20, No. 1, pp. 109–110.

Requicha, A. A., 1983, "Toward a Theory of Geometric Tolerancing," *The International Journal of Robotics Research,* Vol. 2, No. 4, pp. 45–60.

Resnikoff, H. L., 1992, "Wavelets and Adaptive Signal Processing," *Optical Engineering,* Vol. 31, No. 6, pp. 1229–1234.

Rioul, O., and Vetterli, M., 1991, "Wavelets and Signal Processing," *IEEE Signal Processing Magazine,* pp. 14–38.

Sen, A., and Srivastava, M., 1990, *Regression Analysis: Theory, Methods, and Applications* Springer-Verlag, New York.

Shah, J., and Miller, D., 1989, "A Structure for Supporting Geometric Tolerances for Computer Integrated Manufacturing," *Proceedings of the ASME Annual Meeting,* pp. 344–351.

Srinivasan, R. S., 1994, "A Theoretical Framework for Functional Form Tolerances in Design for Manufacturing," Ph.D. thesis, The University of Texas, Austin, TX.

Srinivasan, R. S., and Wood, K. L., 1992a, "A Computational Investigation into the Structure of Form and Size Errors Based on Machining Mechanics," *Advances in Design Automation 1992,* Vol. 1, pp. 161–171, Phoenix, AZ, ASME.

Srinivasan, R. S., and Wood, K. L., 1992b, "Fractal-Based Geometric Toleranc-ing in Mechanical Design," *Proceedings of the 1992 ASME DTM Conference,* pp. 107–115 Phoenix, AZ.

Srinivasan, R. S., and Wood, K. L., 1995, "Geometric Tolerancing in Mechanical Design Using Fractal-Based Parameters," ASME JOURNAL OF MECHANICAL DESIGN, Vol. 117, No. 1, pp. 203–205.

Srinivasan, R. S., Wood, K. L., and McAdams, D., 1996, "A Methodology for Functional Tolerancing in Design for Manufacture," *Journal of Research in Engineering Design,* Vol. 8, No. 2, pp. 99–115.

Stupak, P. R., Syu, C. Y., and Donovan, J. A., 1992, "The Effect of Filtering Profilometer Data on Fractal Parameters," *Wear,* Vol. 154, No. 1, pp. 109–114.

Tipnis, V. A., ed., 1992, *Tolerance and Deviation Information,* New York, ASME CRTD-15-1.

Turner, I. Y., Srinivasan, R. S., and Wood, K. L., 1995, "Investigation of Characteristic Measures for the Analysis and Synthesis of Precision-Machined Surfaces," *SME Journal of Manufacturing Systems,* Vol. 14, No. 5, pp. 378–392.

Turner, J. U., and Wozny, M. J., 1990, "The M-Space Theory of Tolerances," *Advances in Design Automation, 1990–Vol 1.,* Ravani, B. ed., pp. 217–225. ASME.

Vasseur, H., Kurfess, T., and Cagan, J., 1993, "Optimal Tolerance Allocation for Improved Productivity," *Proceedings of the 1993 NSF Design and Manufacturing Systems Conference,* pp. 715–719 Charlotte, NC. NSF, SME.

Walker, R. K., and Srinivasan, V., 1993, "Creating a Standard: Y14.5.1," *Quality,* Vol. 32, pp. 24–28.

Wardle, F. P., 1988, "Vibration Forces Produced by the Waviness of the Rolling Surfaces of Thrust Loaded Ball Bearings–Parts 1 and 2," *Proceedings of the Institution of Mechanical Engineers,* Vol. 202, No. C5, pp. 305–319.

Whitehouse, D. J., 1978, "Surfaces—A Link between Manufacture and Design," *Proceedings of the Institution of Mechanical Engineers,* Vol. 192, pp. 179–188.

Whitehouse, D. J., and Vanherck, P., 1972, "Survey of Reference Lines in the Assessment of Surface Texture," *Annals of the CIRP,* Vol. 21, No. 2, pp. 267–273.

Wick, C., ed.., 1987, *Measurement of Circularity* (4th edition), Vol. IV of *Tool and Manufacturing Engineers Handbook,* Chap. 4, pp. 4.27–4.32, Society of Manufacturing Engineers, Dearborn, Michigan.

Wornell, G. W., 1991, "Synthesis, Analysis, and Processing of Fractal Signals," Tech. rep. 566, Massachusetts Institute of Technology, Cambridge, MA.

Zhang, H. C., and Huq, M. E., 1992, "Tolerancing Techniques: The State-of-the-Art," *International Journal of Production Research,* Vol. 30, No. 9, pp. 2111–2135.